Mitochondrion 81 (2025) 102007

Contents lists available at ScienceDirect

Mitochondrion

journal homepage: www.elsevier.com/locate/mito

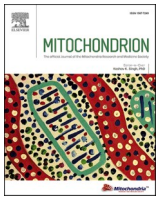

Original Research Article

Novel intronic variant in *NDUFS7* gene results in mitochondrial complex I assembly defect with early basal ganglia and midbrain involvement with progressive neuroimaging findings

Jaakko Oikarainen [a,b,*,1], Reetta Hinttala [a,c,d,1], Naemeh Nayebzadeh [a,c], Salla M. Kangas [a,c], Katariina Mankinen [e], Elisa Rahikkala [a,c,f,g], Hannaleena Kokkonen [a,h], Päivi Vieira [a,c,i], Maria Suo-Palosaari [a,b,j,2], Johanna Uusimaa [a,c,i,2]

[a] *Medical Research Center Oulu, University of Oulu and Oulu University Hospital, Oulu, Finland*
[b] *Research Unit of Health Sciences and Technology, University of Oulu, Oulu, Finland*
[c] *Research Unit of Clinical Medicine, University of Oulu, Oulu, Finland*
[d] *Biocenter Oulu, Oulu, Finland*
[e] *Clinic of Paediatric Neurology, Länsi-Pohja Central Hospital, Kemi, Finland*
[f] *Department of Clinical Genetics, Oulu University Hospital, Oulu, Finland*
[g] *Department of Genomics, Turku University Hospital, Turku, Finland*
[h] *Laboratory of Genetics, Northern Finland Laboratory Centre, Oulu, Finland*
[i] *Clinic for Children and Adolescents, Pediatric Neurology Unit, Oulu University Hospital, Oulu, Finland*
[j] *Department of Diagnostic Radiology, Oulu University Hospital, Oulu, Finland*

ARTICLE INFO

Keywords:
NDUFS7
Leigh syndrome
Rare variant
Neuroimaging
Mitochondrial
Intronic variant

ABSTRACT

Leigh syndrome is the most common phenotype of mitochondrial disorders in children. This study demonstrates clinical, neuroradiological, and molecular genetic findings in siblings with Leigh syndrome and isolated complex I assembly defect associated with intronic c.16 + 5G > A variant in the *NDUFS7* gene. Whole exome sequencing was carried out to identify the causative variant. The gene and protein expression of *NDUFS7* were studied using patient-derived fibroblasts. Assembly of mitochondrial respiratory chain enzymes was analyzed using Blue Native PAGE. This study shows that the *NDUFS7* c.16 + 5G > A variant (rs375282422) has a causative role in Leigh syndrome. Evolution of neuroimaging findings related to this gene variant are demonstrated.

1. Introduction

Leigh syndrome, or subacute necrotizing encephalomyelopathy, is a progressive early-onset neurodegenerative disease, which is the most common clinical presentation of mitochondrial disorders in children, manifesting in infancy or early childhood. (Leigh, 1951; Rahman, 2023) In brain magnetic resonance imaging (MRI), Leigh syndrome is mainly characterized by symmetrical lesions in basal ganglia and brainstem, as well as abnormalities in midbrain, thalami, brainstem, spinal cord, cerebellum, and cerebral white matter. (Haas and Dietrich, 2004; Mascalchi et al., 2018) These lesions show demyelination, gliosis, necrosis, spongiosis, and vascular proliferation. (Cavanagh and Harding, 1994; Alves et al., 2020).

Pathogenic variants in around 100 genes encoded by mitochondrial DNA (mtDNA) and nuclear DNA (nDNA) have been described as associated with Leigh syndrome. (Rahman, 2023; Lake et al., 2016) Complex I deficiency is the leading biochemical basis of Leigh syndrome. (Fernandez-Vizarra and Zeviani, 2021) Complex I, NADH:ubiquinone oxidoreductase, catalyzes the first step in the mitochondrial respiratory chain. (Moser et al., 2006) It is the largest of the four mitochondrial respiratory-chain complexes. (Baradaran et al., 2013; Sazanov, 2023) The core of complex I is composed of 14 subunits that are involved in the

* Corresponding author at: Medical Research Center Oulu, PO Box 50, 90029 OYS, Finland.
E-mail addresses: jaakko.oikarainen@student.oulu.fi (J. Oikarainen), reetta.hinttala@oulu.fi (R. Hinttala), salla.kangas@oulu.fi (S.M. Kangas), katariina.mankinen@mehilainen.fi (K. Mankinen), elisa.rahikkala@oulu.fi (E. Rahikkala), hannaleena.kokkonen@nordlab.fi (H. Kokkonen), paivi.vieira@oulu.fi (P. Vieira), maria.suo-palosaari@fimnet.fi (M. Suo-Palosaari), johanna.uusimaa@oulu.fi (J. Uusimaa).
[1] Shared first authorship.
[2] Shared last authorship.

https://doi.org/10.1016/j.mito.2025.102007
Received 24 September 2024; Received in revised form 26 January 2025; Accepted 30 January 2025
Available online 31 January 2025

energy transduction by oxidizing NADH, reducing ubiquinone and translocating protons through the inner membrane. The remaining 31 proteins, which assemble around the core domains, are supplementary subunits that are likely involved in the assembly, stability, regulation, and protection of complex I against oxidative stress. (Sazanov, 2023; Fiedorczuk et al., 2016; Stroud et al., 2016).

Previous studies have reported only a few children with mitochondrial complex I deficiency manifesting as Leigh syndrome, nuclear type 3 (MC1DN3, OMIM #618224), harboring homozygous or compound heterozygous pathogenic variants in the *NDUFS7* gene on chromosome 19p13. (Triepels et al., 1999; Smeitink and Van Den Heuvel, 1999; Lebon et al., 2007; Lebon et al., 2007) Here, we report two siblings with Leigh syndrome and isolated complex I assembly defect associated with an intronic variant c.16 + 5G > A in the *NDUFS7* gene. Brain MRIs of the siblings are analyzed in detail and the findings are compared to previously published cases of Leigh syndrome.

2. Materials and methods

2.1. Study patients

The index patient (Patient 1) and his younger brother (Patient 2) were examined at Länsi-Pohja Central Hospital and the Unit of Child Neurology at Oulu University Hospital, Finland. Written informed consent was obtained from the parents of the patients. The study protocols concerning the research on patient samples were approved by the Ethics Committee of the Northern Ostrobothnia Hospital District (approved 16 June 2008, and the amendments approved 16 September 2011, and 24 March 2014).

2.2. Brain magnetic resonance imaging

The primary brain MRI of both patients were performed at Länsi-Pohja Central Hospital with the Signa 1.5 Tesla (GE Healthcare, Milwaukee, WI, USA) scanner and the follow-up imaging of both patients at Oulu University Hospital with the Magnetom Espree 1.5 Tesla and Sola 1.5 Tesla (Siemens, Erlangen, Germany) scanners. The imaging protocol included diffusion-weighted imaging (DWI), T1-weighted (T1W) images in sagittal and coronal planes, T2-weighted (T2W) axial images and T2W fluid attenuated inversion recovery (FLAIR) axial images (slice thickness 4–6 mm and a gap of 0.5–1.5 mm). Contrast-enhanced T1W axial sequences were obtained in Patient 1 using gadolinium contrast agent (Gadoteric acid, Dotarem®, 0.2 ml/kg, Guerbet, France). Single voxel short echo-time (30 ms) magnetic resonance spectroscopy (MRS) was performed on Patient 1 at follow-up imaging from the basal ganglia and parietal white matter. The children were sedated during imaging. MRI scans were evaluated using a research PACS/DICOM viewing application for diagnostic radiology (Neaview, Neagen, Helsinki, Finland). The brain MRI abnormalities were evaluated and classified by a pediatric radiologist (JO, with 6 years of radiology experience, and MS-P, with 16 years of radiology and 10 years of pediatric neuroradiology experience).

2.3. Whole exome sequencing

Exome and mitochondrial genome sequencing of both siblings and their parents were performed as part of commercial clinical diagnostics in Centogene AG (Rostock, Germany), as described previously (Trujillano et al., 2017). In brief, the SureSelect Human All Exon V6 kit (Agilent, Santa Clara, CA, USA) was used for enrichment, and a HiSeq4000 (Illumina) instrument was used for the actual sequencing, with the average coverage targeted to 100×. An in-house bioinformatics pipeline was used for base calling, alignment of reads to GRCh37/hg19 genome assembly, primary filtering out of low-quality reads and probable artifacts, and subsequent annotation of variants. All disease-causing variants reported in the Human Gene Mutation Database (Stenson et al., 2017), in Clinvar, or in CentoMD® (Trujillano et al., 2017), and variants with a minor allele frequency of less than 1 % in the gnomAD database were considered. The evaluation was focused on coding exons along with flanking +/- 20 intronic bases. Selected candidate variants were classified according to American College of Medical Genetics and Genomics (ACMG) guidelines. (Richards et al., 2015).

2.4. Sanger sequencing

Total genomic DNA was extracted from the patients' blood samples using the QIAamp DNA Blood Mini Kit (Qiagen, Hilden, Germany). The genomic region of *NDUFS7* was amplified by PCR using Phire II Hotstart polymerase andprimers listed in Supplementary Table 1. The purified DNA fragments were analyzed with Sanger sequencing using an Applied Biosystems 3500xl genetic analyzer (Biocenter Oulu Sequencing Center, Oulu, Finland). The sequencing primers were the same as those used for the amplification of PCR fragments. Sequences were analyzed using Sequencher 4.1.4 (Gene Codes Corporation, Ann Arbor, MI, USA).

2.5. Cell culture

Fibroblast cultures were established from skin biopsies at Oulu University Central Hospital. Fibroblasts were immortalized using a retroviral vectors expressing E7 region of type 16 human papilloma virus and the protein component of human telomerase by the Shoubridge laboratory at the McGill University, Montreal, Canada. (Yao and Shoubridge, 1999) Immortalized fibroblasts were cultured at 37 °C and 5 % CO2 high-glucose DMEM with 100 U/ml penicillin, 100 µg/ml streptomycin, and 10 % FBS (Thermo Fisher Scientific).

2.6. Reverse transcription and Sanger sequencing of the NDUFS7 transcript

Given that the variant of interest was detected in an RNA splicing site between exons 1 and 2, reverse transcription, PCR, and subsequent Sanger sequencing were done to study the integrity and splicing of *NDUFS7* mRNA in patient-derived immortalized fibroblasts. RNA was extracted from the cultured fibroblasts using the RNeasy Plus Mini Kit (Qiagen, Hilden, Germany). A One-Step RT-PCR kit (Qiagen) and primers listed in Supplementary Table 2 were used to amplify and perform Sanger sequencing of the *NDUFS7* transcript as described above.

2.7. RT-qPCR to study the expression level of NDUFS7

The expression level of the *NDUFS7* transcript in the patient-derived immortalized fibroblasts was studied using quantitative reverse transcription PCR (RT-qPCR). Immortalized fibroblasts derived from a healthy donor were used as a control. The cell cultures were run in triplicate for the analysis. RNA was extracted from the cultured fibroblasts using the RNeasy Plus Mini Kit (Qiagen, Hilden, Germany). The mRNA was reverse transcribed to cDNA with a QuantiTect Reverse Transcription kit (Qiagen, Hilden, Germany). The qPCR analysis was performed using IQTM SYBR Green Supermix (Bio-Rad, Hercules, CA, USA) and the CFX ConnectTM Real-Time System (Bio-Rad, Hercules, CA, USA) according to the manufacturer's instructions. The TATA-box binding protein (*TBP*) and transferrin receptor (*TFRC*) were used as endogenous reference genes. The primers were designed using NCBI primer blast (Ye et al., 2012) and the qPCR oligo sequences and product lengths are shown in Supplementary Table 3. Two primer pairs for *NDUFS7* were designed, one spanning over the exons 1–3, including the region with the c.16 + 5G > A variant, and the other primer pair was designed to amplify exons 3–4, the region outside the variant.

2.8. SDS-PAGE and immunoblotting

For sample preparation, one dish (diameter of 10 cm) containing

confluent fibroblasts was used. The cell cultures were run in triplicate for the analysis. The cells were solubilized in 1.5 % n-dodecyl maltoside (Sigma-Aldrich, St. Louis, MO, USA) with the protease inhibitor in 1 × phosphate buffered saline (PBS). A total of 20 μg of whole protein extracts were loaded on 4–20 % Mini-PROTEAN® TGX™ precast protein gels (Bio-Rad Laboratories Inc., Hercules, CA, USA). After electrophoresis, the proteins were electroblotted onto nitrocellulose membranes (Bio-Rad Laboratories Inc., Hercules, CA, USA). The blots were probed by the following primary antibodies: NDUFS7 (PA5-19343, Thermo Fisher Scientific, Waltham, MA, USA) and GAPDH (GTX100118, GeneTex, Irvine, CA, USA). Horseradish peroxidase (HRP)-conjugated secondary antibodies were used to visualize the antibody binding (goat anti-rabbit IgG H&L HRP [Abcam ab97080, 1:10,000] and rabbit anti-goat IgG H&L HRP [Invitrogen #81–1620, 1:10,000]), and the protein bands were detected by ECL chemiluminescent reagents (Advansta, CA, USA). Chemiluminescence detection was conducted using an LAS-3000 Luminescent Image Analyser (Fuji Photo Film, Tokyo, Japan).

2.9. Blue native PAGE

The expression level and assembly of mitochondrial enzyme complexes were analyzed using blue native PAGE (BN-PAGE). The cells were collected and suspended in 1 × PBS without calcium and magnesium from one confluent petri dish (diameter of 10 cm). The sample preparation was done as described previously. (Leary and Sasarman, 2009) A total of 20 μg of detergent-solubilized protein samples were loaded on a 6–15 % acrylamide blue native gradient gel. The gel was run with blue cathode buffer (15 mM Bis-Tris, 50 mM tricine, 0.02 % Brilliant Blue G, pH 7), colorless cathode buffer (without Brilliant Blue G), and anode buffer (50 mM Bis-Tris, pH 7). (Nijtmans et al., 2002; Ugalde et al., 2004) Blots were probed by the following primary antibodies: SDHA (#ab14715), UQCRC2 (#ab14745), COXIV (#ab14744), ATP5A (#ab14748, Abcam), and NDUFA9 (#A21344, Life Technologies). HRP-conjugated secondary antibody (goat anti-rabbit IgG H&L HRP [Abcam ab97080, 1:10,000] and goat anti-mouse IgG H&L HRP [Abcam ab6789, 1:10,000]) was used for immunoblotting as described above.

2.10. Statistical analysis

The assays were performed with three separate sample preparations, and the mean of these samples was calculated. The statistical significance of the difference in the means of RNA expression levels and protein levels was calculated using the Student's *t*-test, assuming unequal variances. Fiji software was used to determine the relative band intensities after immunoblotting of SDS-PAGE and BN-PAGE gels. (Schindelin et al., 2012).

3. Results

3.1. Clinical findings

Patient 1 was the first child of the Finnish parents, born at term with Apgar scores of 9/9/9, weighing 3502 g. His development was initially normal: at 12 months of age, he was able to walk with support and express his first words. His motor development stalled thereafter, and regression was notable at 15 months of age. He showed generalized dystonia, distal spasticity, and axial hypotonia. Deep tendon reflexes were exaggerated and could be elicited over a wide area, with left predominance. Extensor plantar reflex was present on the left. His condition deteriorated rapidly. At 19 months, he could not move independently, and a month later, a gastrostomy tube had to be inserted for feeding. He had severe scoliosis and one severe episode of pneumonia complicated by an empyema at the age of 8. Epilepsy was diagnosed at the age of 10. Since the intrathecal baclofen (ITB) treatment was considered, brain and spinal cord imaging was conducted at the age of 11 years. At 12 years of age he was completely dependent on assistance in all activities of daily living. General dystonia and spasticity had increased, and he had no purposeful limb movements. He was incapable of verbal communication and had significant difficulties with head control. He could shortly fix his gaze on objects but was not able to follow them with his eyes. Peroral baclofen and tizanidine at their maximum doses were insufficient to ease his painful spasticity. ITB pump was implanted with significant benefit.

Patient 2 was the younger brother of Patient 1. He was born full-term following an uncomplicated pregnancy. His weight was 3850 g and Apgar scores 9/9/9. His development progressed normally until 15 months of age, when he was able to walk with support and express his first words. At that age, mild signs of dystonia and distal spasticity of the lower limbs were first noted by his parents. His motor and speech development started to regress.

At the age of 17 months, he was able to crawl but could not stand without help. He showed dystonia, distal spasticity, and axial muscle hypotonia; his tendon reflexes were brisk with predominance on the right side. Extensor plantar reflexes were negative. His condition deteriorated rapidly. At 24 months of age, he was unable to move independently. A gastrostomy for feeding was inserted a month later.

At the age of 7 years he was diagnosed with epilepsy. Spasticity and dystonia were prominent. He could still follow objects by gaze and moving his head. Otherwise, he communicated by facial expressions and eye movements. Intrathecal baclofen treatment was considered, as the peroral treatments for spasticity were insufficient at their maximum doses. Brain and spinal MRI was performed preoperatively.

Neither of the patients needed tracheostomy at the time of latest clinical evaluation at 13 and 8 years of age.

3.2. Laboratory findings

Metabolic workup was conducted on Patient 1 at 18 months of age. Liver transaminases, creatine, ammonia, creatine kinase, urine organic acids, urine oligosaccharides, plasma and urine amino acids were all within normal range. Plasma lactate was 1.57 mmol/l (reference range 0.33–1.33) and plasma pyruvate 97 μmol/l (reference range 40–80). Cerebrospinal fluid lactate was elevated at 2.7 mmol/l (reference range 1.2–2.1).

3.3. Brain MRI findings

3.3.1. Patient 1

Patient 1′s primary brain MRI at the age of 15 months showed swollen basal ganglia and thalami (Fig. 1, Panel 1C). There were symmetrical T2 hyperintensities in the basal ganglia, thalami, midbrain, and brain stem (Fig. 1, Panels 1A–C). The lesions of the globus pallidus showed ring enhancement only on the primary MRI (Fig. 2, Panel 1). At the follow-up T2W axial MRI 7 months later, the basal ganglia and thalami were slightly smaller than in the primary imaging, indicating reduced edema (Fig. 1, Panel 2C). There were progressive signal abnormalities in the putamen, body of the nucleus caudatus and nucleus dentatus (Fig. 1, Panels 2A, 2C, and 2D). Subtle abnormalities of the thalami and dorsal brain stem vanished without atrophy (Fig. 1, Panels 2A and 2C). The lesions of the globus pallidus, substantia nigra, subthalamic nucleus, and tegmentum were smaller, with more T2 hyperintensity (Fig. 1, Panels 2B and 2C) and T1 hypointensity suggesting necrosis. There were no signs of restricted diffusion of the abnormalities or cortical stroke-like lesions. White matter abnormalities were absent.

The follow-up MRI of Patient 1 at the age of 11 years showed markedly progressive cortical signal abnormalities and atrophy (Fig. 1, Panel 3). The diffusion-weighted imaging (Fig. 1, Panel 3A), apparent diffusion coefficient map (Fig. 1, Panel 3B), and T2W images (Fig. 1, Panel 3C–D) showed multiple cortical signal lesions in all lobes, some of them presenting restricted diffusion on apparent diffusion coefficient map demonstrating cytotoxic edema (Fig. 1, Panel 3B). The basal ganglia and thalami presented with progressive T2 hyperintense lesions and atrophy. There were also bilateral signs of necrotic cystic lesions in

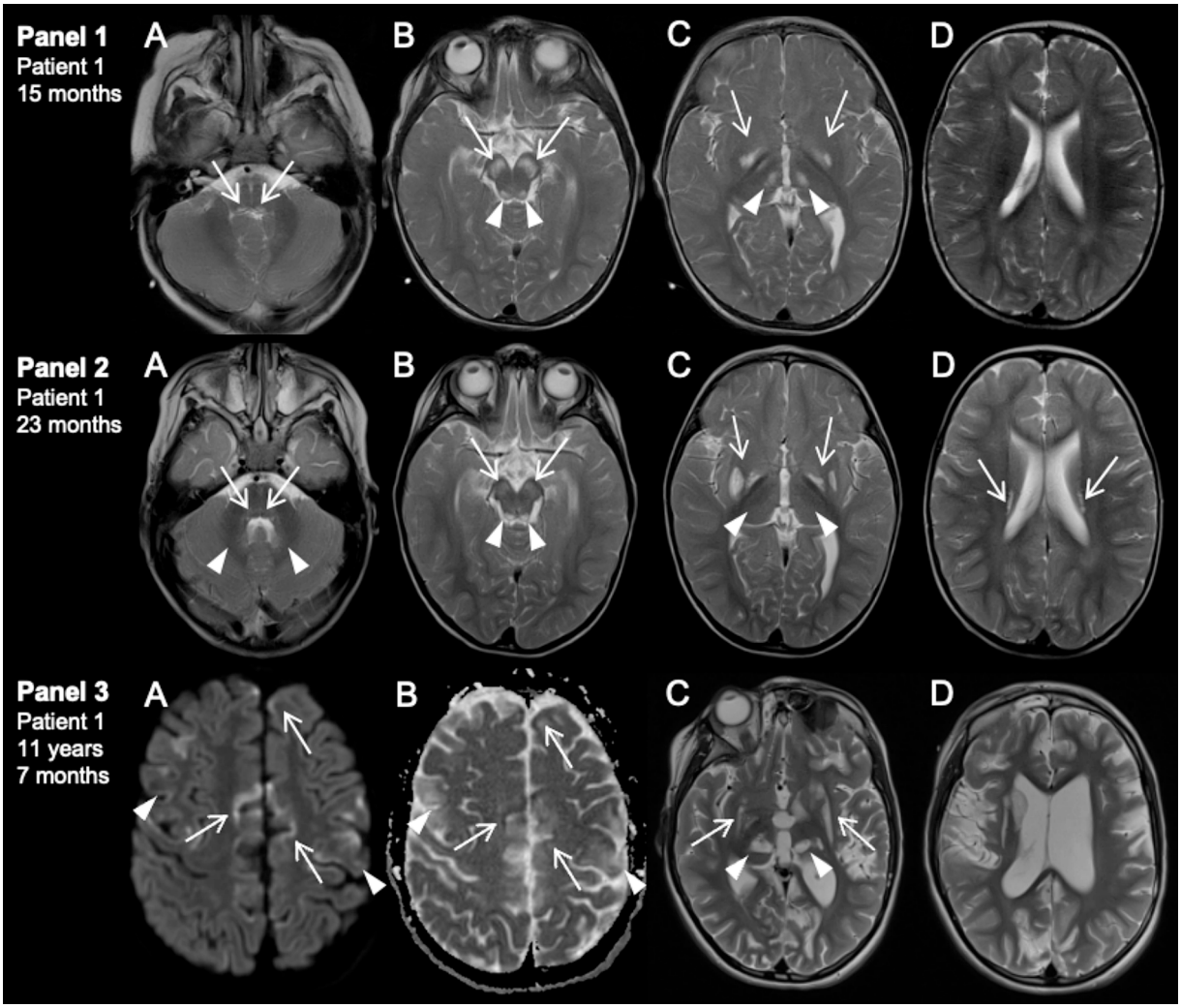

Fig. 1. Brain magnetic resonance images (MRIs) of Patient 1 at the age of 15 months (Panel 1), at the age of 23 months (Panel 2), and at the age of 11 years and 7 months (Panel 3).
Panels 1 and 2: T2-weighted (T2W) axial images show bilateral symmetrical hyperintense lesions of the posterior medulla oblongata at the age of 15 months (1A, arrows), which disappear at the age of 23 months (2A, arrows). Lesions of the substantia nigra and subthalamic nuclei (1B, arrows) and tegmentum (1B, arrowheads) in the midbrain show T2 hyperintensity at the age of 15 months, while they become atrophic at the age of 23 months, suggesting necrosis (2B, arrows and arrowheads). The T2 hyperintense lesions of the nucleus dentatus in the cerebellum are seen at the age of 23 months (2A, arrowheads). Panels 1C and 2C demonstrate T2 hyperintense lesions of the basal ganglia. The lesions of the thalami (1C, arrowheads) and basal ganglia, including the putamen and globus pallidus (1C, arrows), are swollen at 15 months of age. The T2 hyperintensities of the globus pallidus become atrophic at 23 months of age, suggesting necrosis whereas the lesions of the putamen increase at 23 months of age (2C, arrows). The symmetrical medial thalamic T2 hyperintense lesions at the age of 15 months (1C, arrowheads) vanish at the age of 23 months (2C, arrowheads). There are no lesions of the nucleus caudatus at the age of 15 months (1D), while symmetrical hyperintense lesions of the body of the nucleus caudatus are seen at the age of 23 months (2D, arrows).
Panel 3: Diffusion-weighted image (DWI) (3A) and apparent diffusion coefficient (ADC) map 3B demonstrate multiple cortical signal abnormalities with diffusion restriction (3A and 3B, arrows). Some cortical lesions show no diffusion restriction (3A and 3B, arrowheads). Axial T2W image (3C) shows bilateral T2 hyperintense lesions with necrosis in the thalami (3C, arrowheads), and T2 hyperintensity and atrophy of the basal ganglia (3C, arrows). Dilation of the ventricles and cortical subarachnoid spaces are shown in Panel 3D, suggesting progressive atrophy without white matter involvement.

the thalami and lentiform nucleus (Fig. 1, Panel 3C). Susceptibility-weighted imaging presented symmetrical hypointensity in the lentiform nucleus bilaterally, suggesting progressive calcification or metal or hemosiderin deposition. Progressive atrophy involving the white matter, midbrain, brainstem, cerebellum, optic nerves, ventricles, and cortical sulci was present. Subtle T2 signal abnormalities were noted in the hippocampus and midbrain. The cerebellum showed mild atrophy at 11 years of age.

3.3.2. *Patient 2*

The brain MRI of Patient 2 at the age of 21 months demonstrated subtle, symmetrical signal abnormalities in the globus pallidus, midbrain, dorsal brain stem, and cerebellar peduncles surrounding the fourth ventricle on T2W images (Fig. 3, Panels 1A–C). Swollen basal ganglia and prominent bilateral T2 hyperintensities in the putamen and body of the nucleus caudatus were also present (Fig. 3, Panels 1C and 1D). The thalami showed no edema or abnormal hyperintensities. The diffusion of the lesions was not restricted, and there were no cortical stroke-like lesions. White matter abnormalities were absent. A contrast agent was not used.

The follow-up MRI at the age of 7 years and 6 months revealed multiple cortical T2 signal abnormalities on T2W FLAIR axial images with atrophy (Fig. 3, Panels 2A and 2D) but without acute diffusion restriction. Symmetrical T2 signal abnormalities and atrophy were noted in the basal ganglia. Novel symmetrical T2 signal abnormalities appeared in the thalami (Fig. 3, Panel 2C). In the midbrain and

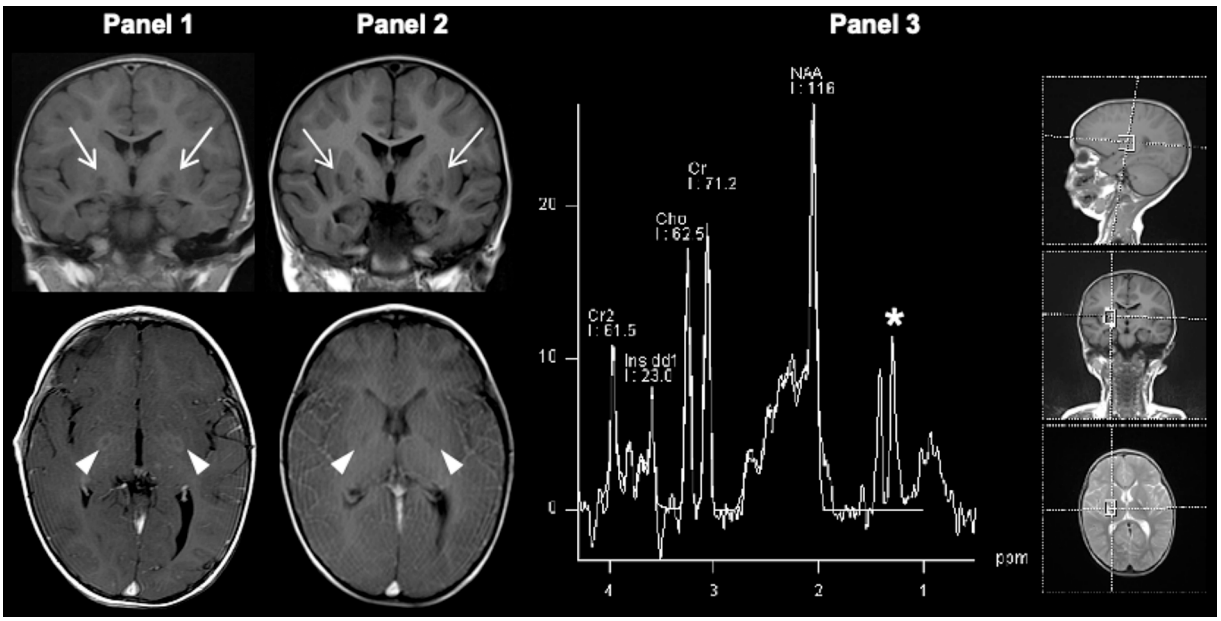

Fig. 2. T1-weighted (T1W) native coronal and contrast-enhanced axial images of Patient 1 at the ages of 15 months (Panel 1) and 23 months (Panel 2). Magnetic resonance spectroscopy (MRS) of Patient 1 at the age of 23 months (Panel 3).
Panel 1 demonstrates slightly hypointense lesions of the globus pallidus on the T1W coronal image (arrows) and ring enhancement (arrowheads) on the T1W axial image with a gadolinium contrast agent.
In Panel 2, the lesions of the basal ganglia are more hypointense on the T1W coronal image, suggesting necrosis (arrows). The lesions do not show contrast enhancement at the age of 23 months (arrowheads).
On Panel 3, the single voxel MRS of the right putamen shows an elevated lactate peak at 1.33 ppm (parts per million magnetic field) (asterisk) at the echo time of 30 ms acquired on a 1.5 T Espree scanner. The N-acetyl-L-aspartate (NAA) peak is normal.

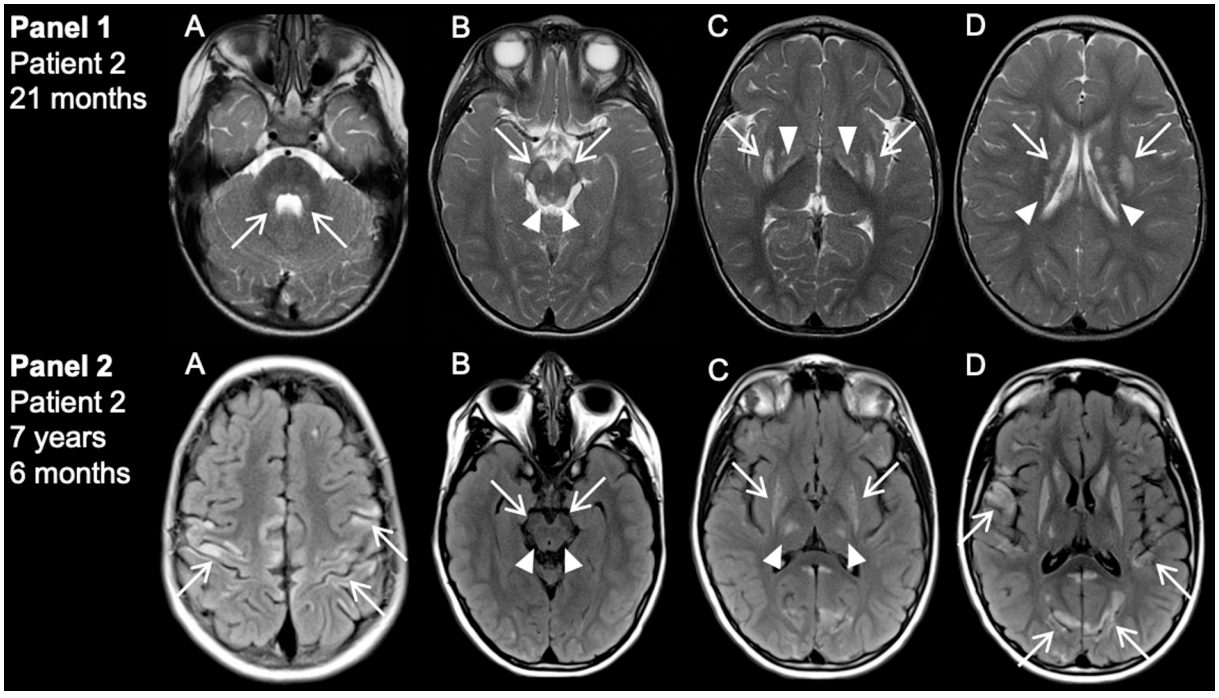

Fig. 3. Panel 1: Axial T2W images of Patient 2 at the age of 21 months. There is mild T2 hyperintensity surrounding the fourth ventricle in the dorsal brainstem and cerebellar peduncles (1A, arrows). Symmetrical T2 hyperintense lesions of the midbrain are located in the tegmentum (1B, arrowheads), substantia nigra, and subthalamic nucleus (1B, arrows). Prominent and swollen T2 hyperintense lesions are demonstrated in the putamina (1C and 1D, arrows) and subtle lesions in the globus pallidus (1C, arrowheads). The bodies of the caudate nuclei show symmetrical T2 hyperintense abnormalities (1D, arrowheads).
Panel 2: Axial T2 FLAIR images of the Patient 2 at the age of 7 years and 6 months. Multiple T2 hyperintense lesions and mild atrophy involve the cortex in all lobes (2A and 2D, arrows). Midbrain lesions in the tegmentum (2B, arrowheads) and in the substantia nigra and subthalamic nucleus (2B, arrows) have vanished. Symmetrical T2 hyperintense lesions are observed in the thalami (2C, arrowheads). Basal ganglia show persistent T2 hyperintense lesions and atrophy (2C, arrows). There is mild cerebral atrophy compared to primary MRI without white matter signal abnormalities (2A–D).

cerebellar peduncles, there was atrophy, but previously detected signal abnormalities in these areas had vanished (Fig. 3, Panel 2B). The cerebral sulci, ventricles, and cerebellum showed mild atrophy, while signal abnormalities in the cerebral white matter were not detected. There were no calcifications on the susceptibility-weighted imaging.

3.4. Molecular findings

Whole exome and subsequent Sanger sequencing of samples from both siblings and their parents revealed an *NDUFS7* c.16 + 5G > A (NM_024407.5, rs375282422) variant, which was initially classified as a variant of unknown significance (Fig. 4A). The variant was identified as a homozygote state in both siblings and as a heterozygote in the parents (Fig. 4B). The c.16 + 5G > A variant resides in *NDUFS7*, which encodes NADH:ubiquinone oxidoreductase core subunit S7 (NDUFS7), a structural subunit for complex I. The rs375282422 variant has been solely observed with an extremely low frequency of 0.0006870 in the Finnish population, indicating a frequency of 0.00002606 worldwide. No homozygotes have been identified. (Database, 2024).

The c.16 + 5G > A is located in a splice-site-region of intron 1 and can therefore affect the mRNA splicing (Fig. 4C). However, the size and nucleotide sequence of the full-length *NDUFS7* mRNA transcript from the patient did not differ from that of the control, suggesting the presence of correctly spliced transcript (Fig. 4D). Next, RT-qPCR was used to quantify the expression level of the *NDUFS7* mRNA using two different primer pairs, one flanking the region containing the variant c.16 + 5G > A. The patient-derived immortalized fibroblasts had significantly lower expression ($p < 0.01$) of the *NDUFS7* transcript amplified by the two primer pairs compared to the control (Fig. 4E), indicating that the c.16 + 5G > A variant has a significant quantitative effect on the mRNA expression. This was confirmed at the protein level by SDS-PAGE and immunoblotting of the patient (II.1) fibroblasts. The results showed a decrease of NDUFS7 protein compared to the control (Fig. 5A), which is in line with the results from qPCR analysis. The assembly of mitochondrial respiratory chain enzyme complexes was then investigated using BN-PAGE. The amount of complex I was dramatically decreased in the patient fibroblasts (II.1) compared to the control fibroblasts indicating significantly impaired assembly process (Fig. 5B).

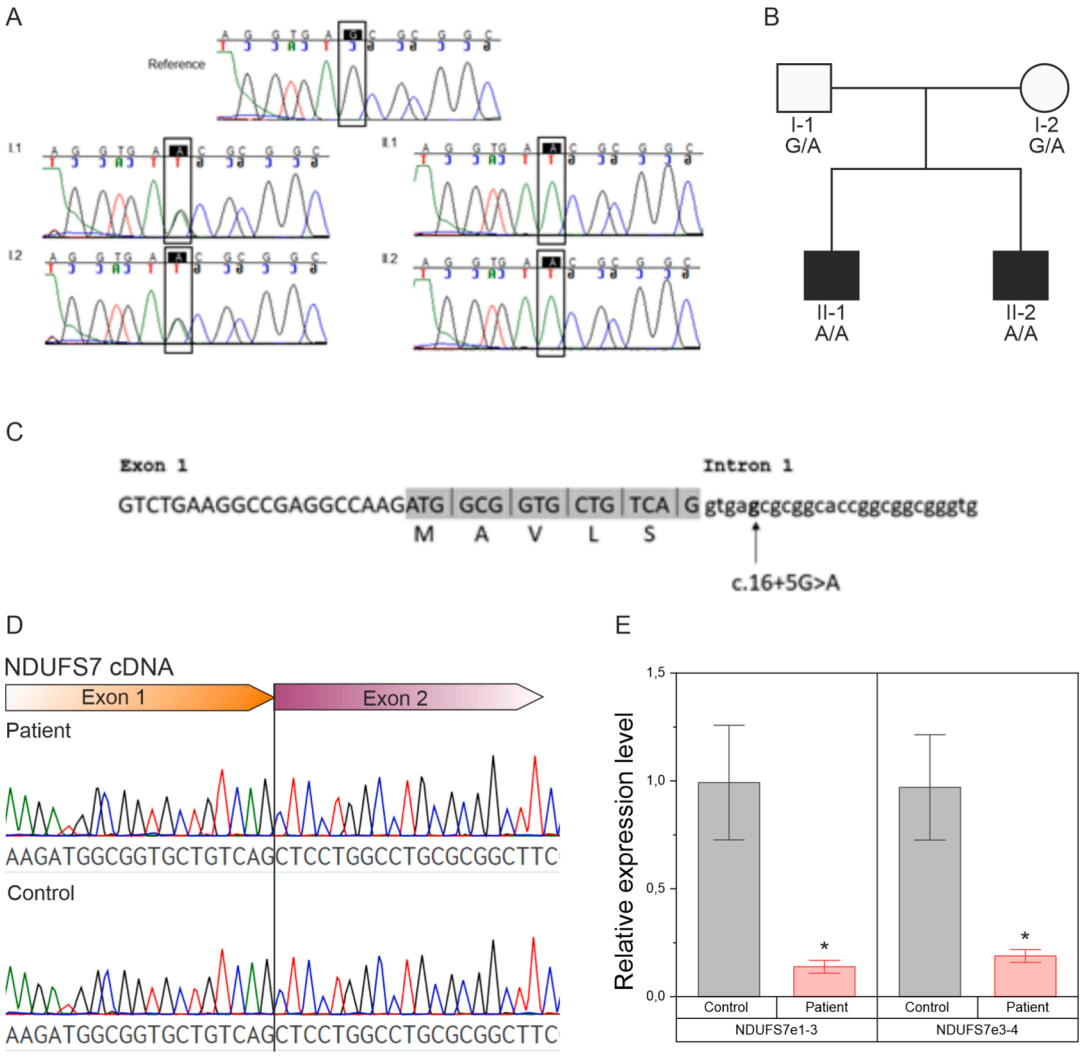

Fig. 4. The siblings are homozygous and the parents are heterozygous carriers for c.16 + 5G > A in *NDUFS7*. **A)** Sanger sequencing confirms the nucleotide change in the family in comparison to the control sequence. The parents are heterozygous carriers for the c.16 + 5G > A variant in the *NDUFS7* gene. Both siblings presenting with Leigh syndrome are homozygous for this variant. **B)** Family pedigree showing affected siblings as shaded squares and their healthy parents. The genotypes are shown next to each family member. **C)** Schematic representation of the variant c.16 + 5G > A in intron 1 of *NDUFS7*. **D)** Full-length *NDUFS7* is amplified from the cDNA of Patient 1 by RT-PCR. Sanger sequencing of the amplified product detects no alterations in the interface of exons 1 and 2 compared to the control. **F)** RT-qPCR analysis of the patient-derived immortalized fibroblasts reveals that the expression level of *NDUFS7* is significantly decreased ($p < 0.01$) compared to the control cell line.

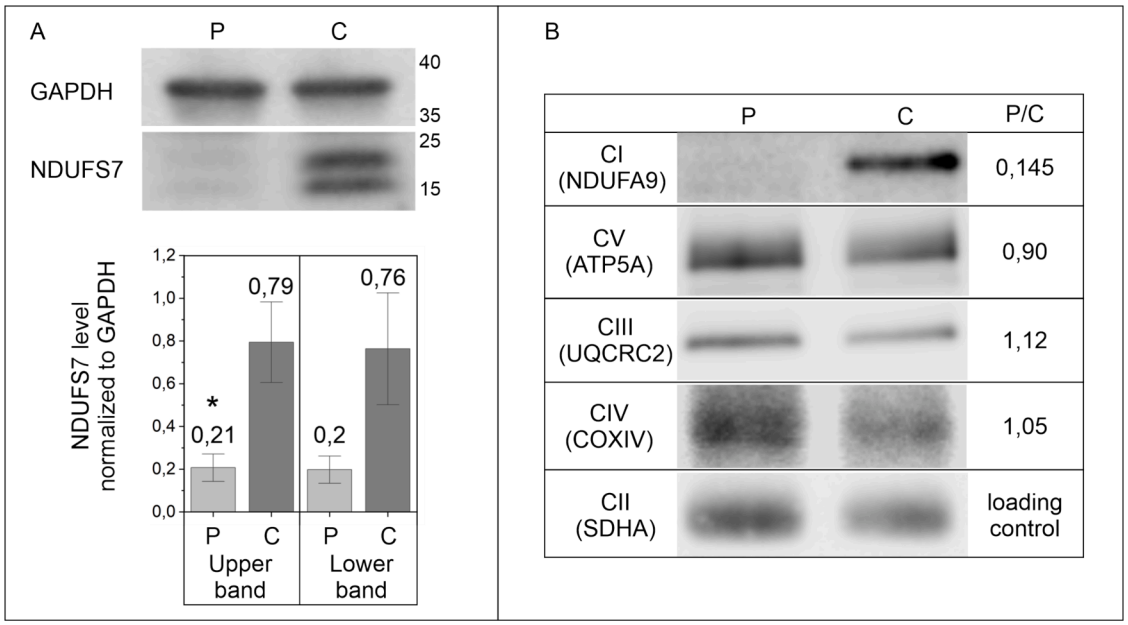

Fig. 5. A) SDS-PAGE analysis showing decreased level of NDUFS7 protein (predicted size 22–24 kDa) in patient (P) fibroblasts compared to control (C). The antibody detects two bands between molecular weight markers of 15 kDa and 25 kDa with intensities shown as numerical values normalized to GAPDH. Both bands are reduced equally in the patient cell line when comparing to the control being 26–27 % of the band intensity of the control. The upper band was changed significantly ($p < 0.05$) compared to control cell line while the change in lower band did not reach statistical significance ($p = 0.058$). **B)** BN-PAGE showing notably decreased amount of complex I (CI) in the patient (P) fibroblasts in comparison to the control (C) while levels of other complexes appear normal.

4. Discussion

We report here two siblings with Leigh syndrome and isolated complex I assembly defect with homozygous intronic c.16 + 5G > A variant in the *NDUFS7* gene. The neuroimaging findings of these patients showed typical abnormalities of the basal ganglia and midbrain, but the brain stem lesions were subtle compared to those previously described patients with Leigh disease caused by complex I deficiency. (Lebre et al., 2011) The patients in this study also showed no white matter signal abnormalities, but the volume of white matter was observed to be slightly decreased in Patient 1 during the 10 years of follow-up. Progression of the cortical and gray nuclei neuroimaging findings of Patient 1 was significant. Neuroimaging findings of the study patients and comparison to literature is presented in the Table 1. The clinical phenotype was neurodegenerative with a combination of dystonia and spasticity that rapidly progressed after 12 months.

Lebon et al. reported a 4-month-old child with another homozygous intronic *NDUFS7* variant (c.17-1167C > G) associated with Leigh disease, who had hyperintensity of the basal ganglia, brainstem, internal capsule, and frontal atrophy, and he died at the age of 5 months. (Lebon et al., 2007) This patient's younger brother had similar symptoms, and he died at 6 months of age. In another study, Lebon et al. demonstrated a 15-month-old child with homozygous *NDUFS7* c.434G > A variant associated with Leigh syndrome. This patient had focal, symmetrical, and necrotic lesions in the thalami, brainstem, and white matter. (Lebon et al., 2007) In another study, two siblings with Leigh disease associated with homozygous NDFUS7 p.V122M variant were reported, with the MRI of another sibling under the age of 5 years showing similar findings as those of the patients in this study, including bilateral lesions of the putamen, nucleus caudatus, nucleus dentatus and brain stem. (Triepels et al., 1999).

Previously cerebellar atrophy has not been reported relating to NDUFS7 variants in children, but it was present in both of our patients. In addition, there were mild hyperintensities of the cerebellar peduncles surrounding the fourth ventricle of the Patient 2 and bilateral hyperintensities in the nucleus dentatus of the Patient 1 as described previously. (Alves et al., 2020; Finsterer and Zarrouk-Mahjoub, 2018).

The findings of our study corroborate the fact that the striatal lesions of the putamen and globus pallidus are common in Leigh disease with complex I deficiency. (Lebre et al., 2011; Danhelovska et al., 2020) The thalamic lesions have only been seen with striatal lesions in a previous report on complex I deficiency. (Lebre et al., 2011) Interestingly, the symmetrical thalamic abnormalities of Patient 1 vanished without atrophy or necrosis at the age of 23 months, while the T2 hyperintense lesions of globus pallidus and midbrain showed cystic necrosis and atrophy. However, cystic necrosis and atrophy in the thalami reappeared at the age of 11 years in Patient 1. Such transitory lesions of basal ganglia and brainstem have been described previously. (Alves et al., 2020) Bilateral symmetric brainstem abnormalities are considered to be usual lesions in the complex I deficiency with striatal hyperintensities, the youngest patient being 4 months of age in a previous study. (Lebre et al., 2011) However, small posterior bilateral lesions of the brainstem were demonstrated at 15 months of age in Patient 1 but, although similar to a previous study by Alves et al., these hyperintensities vanished without necrosis at 23 months of age. (Alves et al., 2020) At the age of 11 years, atrophy and only mild signal abnormalities of the brainstem were noted in Patient 1. Patient 2 had only subtle T2 hyperintensity on the dorsal brainstem at 21 months of age.

The patients in this study had T2 hyperintense lesions of the subthalamic nuclei and tegmentum of the midbrain, which are suggested to be more frequent in patients carrying mtDNA mutations than nDNA mutations. (Lebre et al., 2011) The children with nDNA mutations reportedly present brain abnormalities earlier than those with mtDNA mutations (2.8 years and 8.9 years of age, respectively). (Lebre et al., 2011) However, both nDNA and mtDNA mutations can cause severe early cystic necrotizing leukoencephalopathy with basal ganglia, cerebellum, and brain stem involvement. (Saada et al., 2008; Ogilvie et al., 2005).

Diffusion weighted imaging in Patient 1 at the age of 11 years demonstrated marked cortical involvement. Both acute and chronic cortical ischemia were noted in all lobes based on DWI and T2 FLAIR images. Progression of the lesions in deep gray matter, thalami, and atrophy in multiple structures was remarkable. The majority of patients with complex I deficiency are reported to show an elevated lactate peak

Table 1
Neuroradiological findings in patients with *NDUFS7* variants.

Patients and reference	Age at imaging	Sex (M/F)	Brain MRI signal abnormalities							Other brain MRI abnormalities			
			Brainstem	Putamen	Nucleus caudatus	Globus pallidus	Thalamus	Nucleus dentatus	Midbrain	White matter	Necrotising leukoencephalopathy	Cortical signal abnormalities	Cerebral atrophy	Cerebellar atrophy
Patient 1	15 months – 11 years	M	+	+	+	+	+	+	+			+	+	+
Patient 2	21 months – 7 years	M	+	+	+	+	+		+			+	+	+
Lebre et al., 2011 (29)	11 years	F	+	+		+	+			+	+			
Lebon et al., 2007 (16)	15 months	F	+	+			+			+				
Lebon et al., 2007 (17)	4 months	M	+	+	+	+							+	
Triepels et al., 1999 (14)	<5 years	M	+	+	+			+	+					

in MRS, which suggests the importance of spectroscopy in diagnostics. Patient 1 had a clearly elevated lactate MRS peak in the follow-up image obtained at 23 months of age.

5. Conclusion

To summarize, we show that the intronic *NDUFS7* variant c.16 + 5G > A is a novel recessive cause of complex I assembly defect, leading to Leigh syndrome. Brain MRI demonstrated early symmetrical T2 signal abnormalities and edema in the striatum, midbrain, and brainstem of both patients. However, transitory and fluctuating lesions were detected in serial images, along with simultaneous progressive lesions. Ten years of follow-up showed progressive ischemic cortical and necrotic gray nuclei lesions with severe cerebral and mild cerebellar atrophy. White matter signal abnormalities were not related to this gene variant, as shown in the findings during a relatively long follow-up period, demonstrating the phenotypic variability of *NDUFS7*-related Leigh syndrome.

Ethical statement

The study protocols concerning the research on patient samples were approved by the Ethics Committee of the Northern Ostrobothnia Hospital District (approved 16 June 2008, and the amendments approved 16 September 2011, and 24 March 2014). Written informed consent was obtained from the parents of the patients for the study and publication of the results.

CRediT authorship contribution statement

Jaakko Oikarainen: Writing – review & editing, Writing – original draft, Visualization, Investigation. **Reetta Hinttala:** Writing – review & editing, Writing – original draft, Visualization, Resources, Investigation, Formal analysis, Conceptualization. **Naemeh Nayebzadeh:** Writing – review & editing, Visualization, Resources, Investigation. **Salla M. Kangas:** Writing – review & editing, Writing – original draft, Visualization, Resources, Investigation, Conceptualization. **Katariina Mankinen:** Writing – review & editing, Resources, Investigation. **Elisa Rahikkala:** Writing – review & editing, Resources, Investigation. **Hannaleena Kokkonen:** Writing – review & editing, Resources, Investigation. **Päivi Vieira:** Writing – review & editing, Resources, Investigation. **Maria Suo-Palosaari:** Writing – review & editing, Writing – original draft, Visualization, Supervision, Resources, Project administration, Investigation, Funding acquisition, Conceptualization. **Johanna Uusimaa:** Writing – review & editing, Supervision, Resources, Project administration, Investigation, Funding acquisition, Conceptualization.

Declaration of competing interest

The authors declare that they have no known competing financial interests or personal relationships that could have appeared to influence the work reported in this paper.

Acknowledgments

We acknowledge laboratory technician Pirjo Keränen (University of Oulu, Finland) for her assistance with laboratory experiments on patient-derived cells. We acknowledge the Biocenter Oulu Sequencing Center (University of Oulu, Finland) for its service. This work was supported by the Arvo and Lea Ylppö Foundation, Stiftelsen Alma och K.A. Snellman Säätiö, Oulun Lääketieteellinen Tutkimussäätiö (Oulu Medical Research Foundation), Academy of Finland (JU, decision 331436; RH, decisions no. 311934, 266498, 273790, 303996), Finnish Medical Foundation, Paediatric Research Foundation (RH, JU), and Competitive State Funding for Health Research (JU and MS-P), Oulu University Hospital, Finland. Some authors of this publication are members of the European Reference Network on Rare Neurological Diseases (ERN-

RND), Rare and Complex Epilepsies (EpiCARE), Neuromuscular Diseases (ERN-EURO-NMD), and Rare Congenital Malformations and Rare Intellectual Disability (ERN-ITHACA).

Appendix A. Supplementary data

Supplementary data to this article can be found online at https://doi.org/10.1016/j.mito.2025.102007.

References

Alves, C.A.P.F., Teixeira, S.R., Martin-Saavedra, J.S., et al., 2020. Pediatric Leigh Syndrome: Neuroimaging Features and Genetic Correlations. Ann. Neurol. 88 (2), 218–232. https://doi.org/10.1002/ana.25789.

Baradaran, R., Berrisford, J.M., Minhas, G.S., Sazanov, L.A., 2013. Crystal structure of the entire respiratory complex i. Nature. 494 (7438). https://doi.org/10.1038/nature11871.

Cavanagh, J.B., Harding, B.N., 1994. Pathogenic factors underlying the lesions in Leigh's disease: Tissue responses to cellular energy deprivation and their clinico-pathological consequences. Brain. 117 (6), 1357–1376. https://doi.org/10.1093/brain/117.6.1357.

Danhelovska, T., Kolarova, H., Zeman, J., et al., 2020. Multisystem mitochondrial diseases due to mutations in mtDNA-encoded subunits of complex i. BMC. Pediatr. 20 (1). https://doi.org/10.1186/s12887-020-1912-x.

Genome Aggregation Database. May 3, 2024. https://gnomad.broadinstitute.org.

Fernandez-Vizarra, E., Zeviani, M., 2021. Mitochondrial disorders of the OXPHOS system. FEBS. Lett. 595 (8). https://doi.org/10.1002/1873-3468.13995.

Fiedorczuk, K., Letts, J.A., Degliesposti, G., Kaszuba, K., Skehel, M., Sazanov, L.A., 2016. Atomic structure of the entire mammalian mitochondrial complex i. Nature. 538 (7625). https://doi.org/10.1038/nature19794.

Finsterer, J., Zarrouk-Mahjoub, S., 2018. Cerebral imaging in paediatric mitochondrial disorders. Neuroradiol. J. 31 (6), 596–608. https://doi.org/10.1177/1971400918786054.

Haas, R., Dietrich, R., 2004. Neuroimaging of mitochondrial disorders. Mitochondrion. 4 (5–6 SPEC. ISS.), 471–490. https://doi.org/10.1016/j.mito.2004.07.008.

Lake, N.J., Compton, A.G., Rahman, S., Thorburn, D.R., 2016. Leigh syndrome: One disorder, more than 75 monogenic causes. Ann. Neurol. 79 (2), 190–203. https://doi.org/10.1002/ana.24551.

Leary, S.C., Sasarman, F., 2009. Oxidative phosphorylation: synthesis of mitochondrially encoded proteins and assembly of individual structural subunits into functional holoenzyme complexes. Methods. Mol. Biol. 554. https://doi.org/10.1007/978-1-59745-521-3_10.

Lebon, S., Rodriguez, D., Bridoux, D., et al., 2007. A novel mutation in the human complex I NDUFS7 subunit associated with Leigh syndrome. Mol. Genet. Metab. 90 (4). https://doi.org/10.1016/j.ymgme.2006.12.007.

Lebon, S., Minai, L., Chretien, D., et al., 2007. A novel mutation of the NDUFS7 gene leads to activation of a cryptic exon and impaired assembly of mitochondrial complex I in a patient with Leigh syndrome. Mol. Genet. Metab. 92 (1–2). https://doi.org/10.1016/j.ymgme.2007.05.010.

Lebre, A.S., Rio, M., Faivre D'Arcier, L., et al., 2011. A common pattern of brain MRI imaging in mitochondrial diseases with complex I deficiency. J. Med. Genet. 48 (1). https://doi.org/10.1136/jmg.2010.079624.

Leigh, D., 1951. Subacute necrotizing encephalomyelopathy in an infant. J. Neurol. Neurosurg. Psychiat. 14 (3), 216–221.

Mascalchi, M., Montomoli, M., Guerrini, R., 2018. Neuroimaging in mitochondrial disorders. Essays. Biochem. 62 (3), 409–421. https://doi.org/10.1042/EBC20170109.

Moser, C.C., Farid, T.A., Chobot, S.E., Dutton, P.L., 2006. Electron tunneling chains of mitochondria. Biochim. Biophys. Acta. Bioenerg. 1757 (9–10). https://doi.org/10.1016/j.bbabio.2006.04.015.

Nijtmans, L.G.J., Henderson, N.S., Holt, I.J., 2002. Blue Native electrophoresis to study mitochondrial and other protein complexes. Methods. 26 (4). https://doi.org/10.1016/S1046-2023(02)00038-5.

Ogilvie, I., Kennaway, N.G., Shoubridge, E.A., 2005. A molecular chaperone for mitochondrial complex I assembly is mutated in a progressive encephalopathy. J. Clin. Investigat. 115 (10), 2784–2792. https://doi.org/10.1172/JCI26020.

Rahman S. Leigh syndrome. In: Handbook of Clinical Neurology. Vol 194. ; 2023. doi: 10.1016/B978-0-12-821751-1.00015-4.

Richards, S., Aziz, N., Bale, S., et al., 2015. Standards and guidelines for the interpretation of sequence variants: A joint consensus recommendation of the American College of Medical Genetics and Genomics and the Association for Molecular Pathology. Genet. Med. 17 (5), 405–424. https://doi.org/10.1038/gim.2015.30.

Saada, A., Edvardson, S., Rapoport, M., et al., 2008. C6ORF66 Is an Assembly Factor of Mitochondrial Complex I. Am. J. Hum. Genet. 82 (1), 32–38. https://doi.org/10.1016/j.ajhg.2007.08.003.

Sazanov, L.A., 2023. From the "black box" to "domino effect" mechanism: What have we learned from the structures of respiratory complex i. Biochemical. Journal. 480 (5). https://doi.org/10.1042/BCJ20210285.

Schindelin, J., Arganda-Carreras, I., Frise, E., et al., 2012. Fiji: An open-source platform for biological-image analysis. Nat. Methods. 9 (7). https://doi.org/10.1038/nmeth.2019.

Smeitink, J., Van Den Heuvel, L., 1999. Human mitochondrial complex I in health and disease. Am. J. Hum. Genet. 64 (6). https://doi.org/10.1086/302432.

Stenson, P.D., Mort, M., Ball, E.V., et al., 2017. The Human Gene Mutation Database: towards a comprehensive repository of inherited mutation data for medical research, genetic diagnosis and next-generation sequencing studies. Hum. Genet. 136 (6), 665–677. https://doi.org/10.1007/s00439-017-1779-6.

Stroud, D.A., Surgenor, E.E., Formosa, L.E., et al., 2016. Accessory subunits are integral for assembly and function of human mitochondrial complex i. Nature. 538 (7623). https://doi.org/10.1038/nature19754.

Triepels RH, Van Den Heuvel LP, Loeffen JLCM, et al. Leigh syndrome associated with a mutation in the NDUFS7 (PSST) nuclear encoded subunit of complex I. Ann Neurol. 1999;45(6). doi:10.1002/1531-8249(199906)45:6<787::AID-ANA13>3.0.CO;2-6.

Trujillano, D., Bertoli-Avella, A.M., Kumar Kandaswamy, K., et al., 2017. Clinical exome sequencing: Results from 2819 samples reflecting 1000 families. Eur. J. Human Genetics. 25 (2), 176–182. https://doi.org/10.1038/ejhg.2016.146.

Trujillano, D., Oprea, G.E., Schmitz, Y., Bertoli-Avella, A.M., Abou Jamra, R., Rolfs, A., 2017. A comprehensive global genotype–phenotype database for rare diseases. Mol. Genet. Genomic. Med. 5 (1), 66–75. https://doi.org/10.1002/mgg3.262.

Ugalde, C., Janssen, R.J.R.J., van den Heuvel, L.P., Smeitink, J.A.M., Nijtmans, L.G.J., 2004. Differences in assembly or stability of complex I and other mitochondrial OXPHOS complexes in inherited complex I deficiency. Hum. Mol. Genet. 13 (6). https://doi.org/10.1093/hmg/ddh071.

Yao, J., Shoubridge, E.A., 1999. Expression and functional analysis of SURF1 in Leigh syndrome patients with cytochrome c oxidase deficiency. Hum. Mol. Genet. 8 (13). https://doi.org/10.1093/hmg/8.13.2541.

Ye, J., Coulouris, G., Zaretskaya, I., Cutcutache, I., Rozen, S., Madden, T.L., 2012. Primer-BLAST: a tool to design target-specific primers for polymerase chain reaction. BMC. Bioinformatics. 13. https://doi.org/10.1186/1471-2105-13-134.